Electrochemical fingerprint of archaeological lead silicate glasses from the voltammetry of microparticles approach

Antonio Doménech-Carbó*[a], María-Ángeles Villegas[b], Fernando Agua[b], Sagrario Martínez-Ramírez[e], María Teresa Doménech-Carbó[c], Betlem Martínez[d]

[a] *Departament de Química Analítica. Universitat de València*. Dr. Moliner, 50, 46100 Burjassot (València) Spain.
[b] *Instituto de Historia, CCHS*, CSIC, c/Albasanz, 26-28. 28037 Madrid, Spain
[c]*Institut de Restauració del Patrimoni, Universitat Politècnica de València*, Camí de Vera 14, 46022, València.
[d] Servici d'Investigació Arqueològica Municipal de València, c/Traginers s/n, Polígono Vara de Quart, Valencia, Spain
[e]*Instituto de Estructura de la Materia*, IEM-CSIC, c/Serrano 121, 28006 Madrid

* Corresponding author. E-mail: antonio.domenech@uv.es.

Abstract

The application of a solid-state electrochemical technique, the voltammetry of microparticles (VMP) for studying archaeological lead glass is described. Upon attachment to graphite electrodes immersed into aqueous acetate buffer, characteristic voltammetric profiles were obtained for submicrosamples of archaeological glasses of ages between the 2th and 19th centuries. Bivariate and multivariate chemometric analysis of VMP data permits to characterize individual workshops/provenances allowing a clear discrimination between soda-rich and potash-rich glasses. Analysis of VMP data, combined with XRF, FESEM, AFM and ATR-FTIR and Micro-Raman spectroscopies, denote the presence of Pb(IV) centers accompanying network-former and network-modifier Pb(II).

Keywords: Lead glass; Archaeology; Voltammetry of microparticles; Provenance.

I. Introduction

Glass has played an important role, by both utilitarian and aesthetic reasons, in all periods of History[1,2] so that glass and glazed materials, in particular, lead silicate glasses have been extensively studied in the fields of archaeometry, conservation and restoration of cultural heritage.[3-5] The elucidation of the technology and provenance[6,7] of glass productions is of crucial interest for establishing ethnohistoric, economic and cultural linkages in ancient cultures, so that unexpected linkages,[8] chronology[9] and dating[10] can be derived from analytical data. These studies involve a variety of techniques, involving, apart from well-known electron microscopy, X-ray diffraction and spectroscopic techniques, from isotope analysis[11,12] to synchroton μ-XRF, external-PIXE/PIGE and BSEM–EDS.[13]

Lead silicate glasses have also considerable interest because of their peculiar thermal, optical, and mechanical properties so that their structural chemistry has claimed attention,[14-18] in particular in regard to the leaching of Pb^{2+}.[19,20] In fact, there have been different proposals on the structural role played by lead centers, some of which would act as network modifiers having a sixfold coordinated environment, and others as network formers with a lower coordination number.[18] Recently, Mizuno et al.[21] have proposed a new structural model, which states that lead atoms are linked to another lead by sharing an edge via two oxygen atoms to form a lead-based network constituted by Pb_2O_4 polyhedron units.

In this context, we have applied a solid state electrochemical technique, the voltammetry of microparticles (VMP) for characterizing archaeological lead glass. This technique, developed by Scholz et al.,[22,23] provides analytical information on a variety of insulating, sparingly soluble solids attached to inert electrodes in contact with suitable electrolytes, thus defining a solid-state electroanalysis.[24] Due to the minimal amount of sample required for analytical runs, limited to few nanograms if necessary, this technique is of application for archaeometric purposes.[25] Lead compounds display a well-defined solid state electrochemistry, so that VMP has been applied for authentication, tracing and dating metallic lead based on the voltammetric features of lead corrosion products.[26-28] Additionally, the VMP methodology is able to provide some structural information and a direct information of the oxidation state of electroactive centers so that it was previously applied to the identification of Pb(II) and Pb(IV) in mediaeval glazes[29] and other applications in ceramic materials.[30,31]

Here, we report a VMP study of a series of 15 archaeological lead glass samples from different sites in Spain aimed to test the suitability of this methodology for characterizing technology and provenance data. Studied samples involve both potassium-rich and sodium-rich glasses and cover a period between the Roman age and the 19th century. VMP data are complemented by data from X-ray fluorescence spectroscopy (XRF) and ATR-FTIR and Micro-Raman spectroscopies. The electrochemical response was examined at the nanoscopic scale using field emission scanning electron microscopy-energy dispersive X-ray microanalysis (FESEM-EDX) and atomic force microscopy (AFM) coupled to VMP. This information is also discussed in relation to the problem of the lead coordination in such systems.

II. Experimental

Chemical composition of glass samples were analysed by X-ray fluorescence (XRF). A PANalytical Axios wavelength dispersed X-ray spectrometer equipped with a rhodium tube of 4 kW and 60 kV was used. Analytical determinations were undertaken through the standard-less analytical software IQ+ (PANalytical) from synthetic oxides and natural minerals. XRF analyses were carried out on powdered samples prepared by grinding body glass fragments, with their most external surfaces removed, by polishing in an agate mortar.

Electrochemical experiments were performed at 298±1 K using a CH 920c device (Cambria Scientific, UK) and Ivium CompactStat portable equipment (Ivium Technol. B.V., Eindhoven, The Netherlands) with Pt auxiliary electrode and AgCl (3M NaCl)/Ag reference electrode using aqueous sodium acetate buffer (HAc/NaAc, Panreac) as a supporting electrolyte. In order to test the suitability of in field analysis using portable equipment, no electrolyte degasification was performed. Reference materials were Cu_2O (cuprite), CuO (tenorite), PbO (litharge), PbO_2 (plattnerite), all Merck reagents, accompanied by a synthetic glass named 71PbO (wt. % composition analysed by XRF: $7.64Na_2O$-$1.08Al_2O_3$-$19.74SiO_2$-$0.63K_2O$-0.11CaO-70.80PbO). This glass was melted and annealed in the laboratory at the Instituto de Historia (CCHS, CSIC).

Sample-modified electrodes were prepared by powdering 2-5 μg of sample in an agate mortar and pestle, being subsequently transferred by abrasion to the surface of paraffin-impregnated graphite bars (Staedtler HB, 68% wt graphite) as described in VMP literature.[22,23]

The IR spectra in the ATR mode of the glass samples were obtained using a Vertex 70 (Bruker Optik GmbH, Germany) Fourier-transform infrared spectrometer with an FR-DTGS (fast recovery deuterated triglycine sulphate) temperature-stabilised coated detector and a MKII Golden Gate Attenuated Total Reflectance (ATR) accessory. A total of 32 scans were collected at a resolution of 4 cm^{-1} and the spectra were processed using the OPUS 5.0/IR software (Bruker Optik GmbH, Germany).

Confocal Raman microscope Renishaw Invia equipped with a Leica microscope and an electrically refrigerated CCD camera was used. Laser excitation lines were provided by a Renishaw Nd;YAG laser (532 nm). The laser beam power used was 5 mW. The frequencies were calibrated with silicon. Origin Microcal Software was used to adjust the deconvolution of the Raman spectra curve fitted with Gaussian function.

Samples were examined with a field emission scanning electron microscope (FESEM-EDX) Zeiss model ULTRA 55 operating with an Oxford-X Max X-ray microanalysis system. The analytical conditions were: 20 kV accelerating voltage, and 6-7 mm as working distance. X-ray microanalysis system is controlled by Inca software. Quantitative spot measurements on the different mineral phases and individual grains and aggregates provided their chemical composition. Quantitative microanalysis was carried out using the ZAF method for correcting interelemental effects included in the Inca software. The counting time was 100 s for major and minor elements. In situ AFM-monitored electrochemical experiments were performed with a multimode AFM (Digital Instruments VEECO Methodology Group, USA) with a NanoScope IIIa controller and equipped with a J-type scanner (max. scan size of 150×150×6 μm). The topography of the samples was studied in contact mode. An oxide-sharpened silicon nitride probe Olympus (VEECO Methodology Group, model NP-S) has been used with a V-shaped cantilever

configuration. Transference of sample particles to a carbon plate and experimental conditions were similar to those previously described for studying lead pigments.[32]

III. Results and Discussion

(1) Glass composition

Table 1 summarizes the provenance, chronology and the composition of main elements determined from XRF and SEM/EDX data (expressed as weight percentage of the corresponding oxides) of the archaeological lead glass samples studied (see Supplementary Information for the entire composition data). Following the Brill's model,[4,33,34] the studied glasses can in principle be divided into potash-rich glasses (samples S05, S06, S07 and S10), and soda-rich glasses (S01, S02, S03, S04, S08, S11, S12 and S14), with samples S09 and S13 having intermediate compositions. Although the composition of several samples from the same origin (samples S05 and S06 from Burgo de Osma, S11 and S12 from l'Almoina) presented quite similar compositions, thus suggesting that were prepared in common workshops/age, others, such as samples S01, S02 and S03 from Puxmarina (Figure 1) and S08 and S09 from Goyeneche, provided a relatively large separation in their respective compositions.

On the other hand, the studied samples cover a wide range of possibilities concerning the lead oxide loading of the glass. As can be seen in Table 1, samples S02, S03 and S09 were soda glasses with large lead oxide loadings, whereas samples S05 and S06 corresponded to potash glasses with high percentages of lead oxide. Samples S01, S04, S08 and S11 to S14 contained relatively low lead oxide amounts.

In Figure 2 the Na_2O content of glasses versus their K_2O content is represented. Most of the samples can be classified into two groups, which correspond to soda-rich glasses and potash-rich glasses, regardless their respective PbO percentage. Only samples S09 and S13 can be considered as sodium and potassium mixed glasses and, hence, their position in Figure 2 is not included in the two compositional groups mentioned.

(2) Voltammetric pattern

Figure 3 shows the typical cyclic voltammetric response obtained at sample-modified graphite electrodes in contact with aqueous acetate buffer at pH 4.75. The voltammograms show a cathodic wave near –0.70 V (C_{PbOx}) which, in the light of abundant literature on the electrochemistry of lead compounds,[21,24-27] can be attributed to the reduction of Pb(II) species in the glass. This signal is followed by a rising current at more negative potentials which corresponds to the reduction of hydrogen ions (C_H). In the subsequent anodic scan, a tall peak appears at –0.45 V (A_{Pb}), corresponding to the oxidative dissolution of the deposit of lead metal formed in the precedent cathodic run.[21,24-27] Such processes can be represented as:

$$Pb^{II}O_x\ (glass) + 2xH^+\ (aq) + 2xe^-\ \rightarrow\ Pb\ (solid) + xH_2O \quad (1)$$

$$Pb\ (solid)\ \rightarrow\ Pb^{2+}\ (aq) + 2e^- \quad (2)$$

Repeatability tests were performed for each archaeological specimen from three replicate experiments using freshly sample-modified electrodes; in all cases, as shown in Fig. 3, the voltammetric profile was satisfactorily reproduced with maximum peak potential separations of ±10 mV.

In copper-containing glass (samples S01-S03 from Puxmarina), the voltammetric response was enriched by the appearance of the signals for the reduction of Cu(II) glass species at –0.10 V (C_{CuOx}) accompanied by the corresponding oxidative dissolution of the deposit of Cu metal at 0.00 V (A_{Cu}), as can be seen in Figure 4, where square wave voltammetry, a particularly sensitive technique, was used. This technique permits to separate different cathodic signals in the potential range between –0.45 and –0.75 V, all attributable to reduction processes such as described by Eq. (1) involving lead species having different coordinative environments.

Two general lead-centered features should be underlined which can be clearly seen in Figs. 4a,c: i) a weak additional cathodic signal at +0.70 V (C^*_{PbOx}) appeared; ii) the signal C_{PbOx} exhibits peak splitting, exhibiting overlapping waves between –0.55 and –0.85 V. By the first token, the peak C^*_{PbOx} can be attributed to the presence of Pb(IV) species which are reduced to Pb(II) ones, as described by PbO_2-modified electrodes[35-38] and observed for archaeological metallic lead plates.[26-28]

$$Pb^{IV}O_z\ (glass) + 2yH^+\ (aq) + 2ye^- \rightarrow Pb^{II}O_{z-y}\ (s) + yH_2O \qquad (3)$$

By the second, the appearance of different C_{PbOx} signals can be considered as indicative of the presence of different Pb(II) species in the glass representative of different coordinative environments (*vide infra*). The coexistence of different Pb(II) species was confirmed by the appearance, in several samples, of peak splitting in the oxidative dissolution process A_{Pb}. This feature, according to extensive VMP literature,[22,23] can be attributed to the oxidation of different lead deposits, a feature often observed in the voltammetry of lead pigments.[26-28,38,43,44]

Consistently, AFM examination of glass fragments attached to graphite plates in contact with acetate buffer submitted to reductive potential inputs displayed different habits in regard to the formation of deposits of metallic lead. Figure 5 compares the AFM amplitude error channel graphs of deposits of a soda-rich sample (SP01) and a potash-rich sample (SP05) immobilized onto a graphite plate in contact with aqueous acetate buffer, after application of a reductive potential input of –0.70 V for 3 min. Before the application of the reductive potential, the glass deposits consisted of irregular glass grains which can be easily distinguished from the graphite terraces. After application of a reductive potential input, the soda-rich glass produced a set of irregular grains of metallic lead in the vicinity of the parent glass grain (type 1 deposit), accompanied by globular clusters (type 2 deposit) almost regularly distributed on the surrounding graphite terraces, and also by fine grains (type 3 deposit). This last type of deposit can be seen in FESEM images in Figure 6. In contrast, potash-rich glasses produced only a dense array of fine grains of metallic lead which tends to concentrate near the parent glass grains (type 4 deposit), which become essentially undisturbed.

(3) Micro-Raman characterization

By reasons of disposable amount of samples ATR-FTIR and Raman spectra were obtained for samples S01 to S10. Raman spectra of samples S01, S02, S03, S05, S06, S08 and 71PbO are depicted in Figure 7. Such spectra consist of two groups of overlapping bands between 300 and 600 cm^{-1}, and between 900 and 1300 cm^{-1}. Similar features were obtained in ATR-FTIR spectra (see Supplementary material). The former can be assigned to Si – O – Si bending vibrations within inter – tetrahedral linkages, whereas the later corresponds to Si – O stretching vibrations of mainly depolymerized silicate species. To analyze such spectra, the usual model will be used in which all the cations create 'non-bridging oxygens' (NBOs) within the silicate structure, denoted by Q^n, where *n* is the number of bridging oxygens, so that one can distinguish between the different tetrahedral species in the network: Q^4 to silicate species with no NBO (SiO_2), Q^3 to silicate species with one NBO (Si_2O_5), and Q^2 to silicate species with two NBOs (SiO_3).[47,48] Raman bands at 890, 930, 970, 1030 and 1100 cm^{-1} were attributed to the SiO_4 tetrahedra with 4, 3, 2, 1 non-bridging oxygen ions and with all bridging oxygen ions, respectively (SiO_4^{4-}, $Si_2O_7^{6-}$, $Si_nO_{3n}^{2n-}$, $Si_nO_{5n}^{2n-}$, $Si_{4n}O_{9n}^{2n-}$).[49] Monovalent and polyvalent cations would be ordered differently among the different NBOs. Alkali cations would be preferentially bonded to NBO from Q^3 units, while alkaline-earth or polyvalent cations would be preferentially bonded to NBO from Q^2 units.[50,51]

In this context, Robinet et al.[52] have recently studied lead glasses concluding that the intensity of the 1100 cm^{-1} peak was linearly correlated to the content in alkali and alkaline-earth in the glass and that the shift in the 1070 cm^{-1} band is proportional to the PbO content of the glass whereas the area of the 990 cm^{-1} band relative to the area of the stretching band varied also linearly with the PbO content, in agreement with the idea that this band is associated with the vibration of Q^2 species that are coordinated with lead ions.[53,54] Raman spectra of the samples studied here in the 900 and 1300 cm^{-1} wavenumber region agree with the above scenario. As can be seen as a Supplementary information (see Figure S1), there is correlation between the lead concentration in the glass and the position of the Q^3 units.

Robinet et al.[52] also obtained that the lead content does not influence the intensity of the 1100 cm^{-1} band. This feature supports the idea that the ordering of lead cations is different from the ordering of alkali and alkaline-earth cations.[52] Consistently, the relative intensity of the different bands in the wavenumber region between 900 and 1300 cm^{-1} exhibit different variations depending on the presence of lead. Data for ATR-FTIR bands (see Supplementary information, Figure S2) indicate that the $I(900)/I(max)$ ratio varies monotonically with the $I(1100)/I(max)$ ratio (squares) with relatively low data dispersion, thus suggesting that the 900 and 1100 cm^{-1} bands, although depending on the total alkali content, are non-affected by lead. In contrast, the data for the $I(1030)/I(max)$ ratio exhibited a clearly larger dispersion relative to a monotonic variation with the $I(1100)/I(max)$ ratio, thus suggesting that the 1030 cm^{-1} band was dependent on lead and that this dependence was different for the different tested samples.

Remarkably, the Micro-Raman spectra of lead silicate glasses exhibit intense bands in the 300 to 600 cm^{-1} region, particularly for the synthetic sample 71PbO, in contrast with alkaline glasses with no lead.[56,57] Figure 8 depicts the spectral decomposition of the Micro-Raman spectra of samples S02 and S08. Here, bands at 370, 465, 575 and 635 cm^{-1} can be discriminated. Such bands are close to those recently reported by Burgio et al.[55] for plattnerite (PbO_2, 424, 515 and 653 cm^{-1}), minium (Pb_3O_4, 390 and 546 cm^{-1}), and

litharge (PbO, 551 cm^{-1}).Comparison of such spectra with voltammograms in Figures 9 and 10 reveal that the presence of a predominating contribution of the 465 cm^{-1} band in the Micro-Raman spectra, occurring in samples S01 to S03, S05 and S06 is correlated with a relatively intense voltammetric peak at –0.55 V. For our purposes, the relevant points to emphasize are that: i) Raman spectra present different Pb-O features, some close to that for Pb(IV) species; ii) bands in the Si – O stretching vibrations exhibit different variations depending on the presence of lead suggesting differences between the different samples.

(4) Provenance and technique

To analyze voltammetric data it is pertinent to note that, since the electrode conditioning procedure used in VMP does not allow for controlling the net amount of sample transferred onto the electrode surface, the absolute currents –in spite of satisfactory repeatability, see Figure 3- cannot be directly used for analytical purposes. Then, peak current and/or peak area ratios will be used for characterization purposes.[22-24] Figure 9 compares the cyclic voltammograms, after semi-derivative convolution, of different soda-rich glass samples having low lead oxide loadings, whereas Figure 10 illustrates representative voltammograms for potash-rich glasses. Comparing the voltammetric records with composition data, the observed regularities can be summarized as follows:

a) The lead oxide loading determines to a great extent the general structure of the glass. Regardless their soda-rich or potash-rich character, Pb-rich (PbO loading up to ca. 10%) samples display significant splitting in the C_{PbOx} signal, in all cases exhibiting a well-defined peak at ca. –0.55 V (see Figs. 4a,c and 10a,b).

b) There is close similarity between the voltammograms of samples from the same provenance. This is the case of S11 and S12 (Figs. 9a,b), both from the l'Almoina archaeological site. Analogously, Goyeneche samples S08 and S09 (Figs. 9e,f) displayed quite similar voltammograms as well as samples S05, S06 from Burgo de Osma (Figs. 10a,b). Possibly, each pair of samples corresponded to an identical manufacturing technique, corresponding to a common provenance and chronological period.

c) In the case of Puxmarina samples, the voltammograms of specimens S01, S02 and S03 (see Figure 11a-c) were clearly similar but exhibiting differences among them. Possibly, considering the amplitude of the Caliphal period in which such samples could be prepared, this case would correspond to different periods and/or provenances but within the same production technique.

In order to establish numerical diagnostic criteria for establishing the common or different provenance/technique of the glass samples, the relative height of the different C_{PbOx} and A_{Pb} peaks were considered. Figure 12 depicts a two-dimensional diagram using the ratios between the current at the –600 mV peak and the maximum current in the C_{PbOx} group of peaks, $i(-600)/i(\max)$, and the ratio between the main anodic peak and the above maximum current, $i(A_{Pb})/i(\max)$. One can see in this diagram how the samples from the same provenance and period, S01, S02, S03 from Puxmarina, S05, S06 from Burgo de Osma and S08, S09 from Goyeneche, fall within a small region of the diagram clearly separated from the regions where other samples appear. This is also the case of samples S10 and S11 from l'Almoina. Interestingly, the data points for the l'Almoina samples, dated in 13^{th}-15^{th}, are close to the data point for sample S13, from Manises, located near to

l'Almoina in the surroundings of the city of Valencia (Spain), but dated in 16^{th}-17^{th}. This feature suggests that the manufacturing technique was maintained in local glass workshops along such historical times.

Hierarchical cluster analysis using voltammetric data was based on peak currents normalized to the larger peak current in square wave voltammograms such as in Figure 4, in agreement with literature.[58] Figure 13 shows the resulting dendrogram (data presented as a Supplementary material) produced a well-defined separation between the glasses from different archaeological sites. In particular, Puxmarina (S01, S02, S03), Burgo de Osma (S05, S06) and l'Almoina plus Manises samples (S11, S12, S13).

(5) Structural considerations

In the traditional view of lead silicate glasses, lead played a dual role as a network former (formally Pb^{4+} replacing Si^{4+}) or as a network modifier.[59] Earlier studies suggest that the existence of PbO_3 or PbO_4 structural units, which act like network formers, may be the reason for the wide formation range of lead-containing glasses, but the structure beyond short-range order is still unclear. Rybicki et al.,[60] based on EXAFS and molecular dynamic studies, suggested that the PbO_4 groups are the dominant structural units in lead-silicate glasses for any concentration and at lower PbO concentrations the co-existence of the PbO_4 and PbO_3 groups is possible. Takahashi et al.[18,21] proposed a structural model, which states that lead atoms are linked to another lead by sharing an edge via two oxygens to form Pb_2O_4 trigonal pyramid units, which would be incorporated into the silicate network as a network former without disturbing the charge balance of the neighboring silicate network. In this view, in the low lead oxide silicate glasses, isolated plumbate units would exist in the silicate network, whereas in the high lead oxide silicate glasses, the lead atoms would construct a glass network and, for intermediate lead loadings, a 3D percolative plumbate network would be formed. More recently, Kohara et al.[61] reported that the network formation in the glass is governed by the interplay of SiO_4 tetrahedra and PbO_x polyhedra (x = 3–5, x = 4 is major) as a network former, while the distribution of other (non-networking) units is inhomogeneous.

Voltammetric data suggest that lead silicate glasses exhibit a significant structural complexity. First of all, characteristic voltammetric features (see Fig. 4), common to those observed for plattnerite[35-38] and corroded metallic lead,[26-28] indicate that some Pb(IV) exists, in agreement with the interpretation of XANES spectra in glazes from decorated tiles of the 16^{th} to 18^{th} century reported by Figueiredo et al.[62] Consistently, Raman data suggest, based on the appearance of the feature at 515 $cm^{-}1$, that Pb(IV) species exists. In fact, as depicted in Figure 14, both Raman data, reflected by the ratio between the intensities of the bands at 515 and 950 cm^{-1}, $I(515)/I(950)$, and voltammetric data, expressed by the ratio between the peak currents for the $C_{Pb(IV)}$ and the maximum current in the C_{PbOx} group of peaks, i(Pb(IV))/i(PbOx), indicate that the amount of Pb(IV) relative to total Pb increases as the Pb loading in the glass increases.

Peak splitting appearing in the cathodic region of the voltammograms of lead silicate glass specimens would be in principle interpreted on the basis of the two extreme models: i) coexistence of Pb(II) centers with different coordinative environments;[45-47] or ii) existence of a unique network-forming coordinative arrangement, based on trigonal Pb_2O_4 units, but

distributed differently.[18,21] In this regard, pertinent voltammetric data can be summarized as:

i) In the cases of litharge,[26-28,30,32,38] where Pb posseses a unique pyramidal four-coordinated environment, and the synthetic glass 71PbO (see Figure 11d), the voltammograms exhibit a unique, isolated cathodic peak at ca. −0.60 V.

ii) In the case of corrosion layers of litharge formed on metallic lead, the main reduction process appearing at potentials between −0.60 and −0.70 V is accompanied by a second signal at potentials between −0.90 and −1.00 V. These signals can be attributed, respectively, to the reduction of the semi-permeable PbO patina, and different layers of porous corrosion products, respectively;[26-28,35-37] i.e., the reduction of 'open' porous structures occur at potentials more negative than those where the reduction of crystalline PbO occurs.

iii) In archaeological lead silicate glasses containing high lead oxide loadings, a tall cathodic signal appears at potentials less negative (−0.50 V, see Figures 12a,b and 11a-c) than those for the ubiquitous reduction process at −0.60 V. The peak at −0.50 V is accompanied by large A_{Pb} peaks and decreases respect to the peak at −0.60 V in the second and successive potential scans. These last features would be consistent with the attribution of this peak to the reduction of network-modifier Pb(II) and would be consistent with the appearance of relatively intense Raman bands at ca. 650 cm^{-1}.

iv) Anodic stripping peaks increased in general on increasing the lead content of the glass being particularly pronounced for potash-rich glasses, while soda-rich glasses frequently exhibited anodic peak splitting.

Consistently, AFM-VMP data produced different types of reductive habits upon applying cathodic potential inputs, mimicking experiments on lead minerals[40] and pigments.[32] The observed AFM and FESEM features can be interpreted on considering that type 1 lead deposit was similar to that observed by Hasse and Scholz[35] in the reduction of litharge. Here, a topotactic conversion of lead oxide into metallic lead occurred so that the lead crystal grows in the vicinity of the parent lead oxide crystal. This kind of process would involve the maintenance of a high structural integrity and could be tentatively associated to the reduction of network-forming trigonal Pb_2O_4 units. Deposits of types 2-4, however, would involve to some extent the release of Pb^{2+} ions and their reduction relatively far from the parent glass grain. As far as the lead deposits of type 2 involve relatively fast nucleation and nucleus growth processes, it can be tentatively attributed to Pb_2O_4–based chains released from the glass. It is no clear if the formation of fine deposits of types 3 and 4 can be attributed to this kind of structural units. Three features should be underlined: i) the parent glass grains remained without apparent morphological damage in the case of type 4 deposits (see Figure 5c,d); ii) the type 3 and type 4 deposits were essentially identical; iii) type 4 deposits were considerably more abundant than type 3 deposits (see Figure 6). These features suggest that these deposits could be attributed to network-modifier Pb^{2+} ions released more easily in the 'open' potash-rich crystals than in soda-rich glass.

Conclusions

Application of the voltammetry of microparticles methodology to submicrosamples of archaeological glasses from different Spanish archaeological sites dated between the 2th and 19th centuries yields well-defined electrochemical responses in contact with aqueous acetate buffer. Characteristic voltammetric profiles were obtained for samples of different sites, thus allowing an electrochemical tracing and discrimination between techniques/workshops/provenances and permits to discriminate between soda-rich and potash-rich glasses.

Analysis of electrochemical data, combined with those from XRF, FESEM, AFM and Micro-Raman spectroscopy, confirms the presence of Pb(IV) centers in the glasses and suggests that the picture of lead glasses as formed exclusively by network-forming trigonal Pb_2O_4 units should be re-examined to consider the presence of both network-former and network-modifier Pb(II).

Acknowledgements: Financial support from the MINECO Projects CTQ2014-53736-C3-1-P, CTQ2014-53736-C3-2-P and HAR2012-30769, which are supported with ERDF funds is gratefully acknowledged. Likewise financial support of Comunidad de Madrid and structural funds of EU through Programa Geomateriales 2 ref. S2013/MIT-2914 is acknowledged. The authors wish to thank the Sección de Investigación Arqueológica Municipal de Valencia for kindly authorizing sampling for carrying out this research. The authors also whish to thank Dr. José Luis Moya López and Mr. Manuel Planes Insausti (Microscopy Service of the Universitat Politècnica de València) for technical support.

References

[1]R. G. Newton and S. Davison, "Conservation of Glass," Butterworth-Heinemann, Oxford (1989).

[2]M. García-Heras, J.M. Fernández-Navarro and M.A. Villegas-Broncano, "Historia del vidrio: desarrollo formal, tecnológico y científico", Proyecto PIE 200460E594, CSIC, Madrid (2012).

[3]W. H. Dumbaugh and J. C. Lapp, "Heavy-Metal Oxide Glasses," *J. Am. Ceram. Soc*. **75**, 2315–2326 (1992).

[4]C. R. Kurkjian and W. R. Prindle, "Perspectives on the History of Glass Composition," *J. Am. Ceram. Soc*. **81**, 795–813 (1998).

[5]O Mecking, "Medieval lead glass in Central Europe," *Archaeometry*, **55**, 640–52 (2013).

[6]R Arletti, G. Vezzalini, C. Fiori and M. Vandini, "Mosaic glass from St Peter's, Rome: Manufacturing techniques and raw materials employed in the late 16th-century Italian opaque glass," *Archaeometry*, **53**, 364–86 (2011).

[7]N Schibille, P. Degryse, M. O'Hea, A. Izmer, F. Vanhaecke and J. McEnzie, "Late Roman glass from the 'Great temple' at Petra and Khirbet Et-Tannur, Jordan-Technology and provenance," *Archaeometry*, 54, 997–1022 (2012).

[8]J. Vargerg, B. Gratuze and F. Kaul, "Between Egypt, Mesopotamia and Scandinavia: Late Bronze Age glass beads found in Denmark," *J. Archaeol Sci*., 54, 168–81 (2015).

[9]J. J. Kunicki-Goldfinger, I. C. Freestone, I. McDonald, J. A. Hobot, H. Gilderdale-Scott and T. Ayers, "Technology, production and chronology of red window glass in the medieval period – rediscovery of a lost technology," *J. Archaeol. Sci*., **41**, 89–105 (2014).

[10]C. M. Stevenson, M. Gleeson and S. W. Novak, "The surface hydration of soda-lime glass and its potential for historic glass dating," *J. Archaeol. Sci*., **52**, 293–9 (2014)

[11]J. Henderson, J. A. Evans, H. J. Sloane, M. J. Leng and C. Doherty, "The use of oxygen, strontium and lead isotopes to provenance ancient glasses in the Middle East," *J. Archaeol. Sci*., **32**, 665–73 (2005).

[12]A. G. Nord, K. Billström, K. Tronner and K. B. Olausson, "Lead isotope data for provenancing mediaeval pigments in Swedish mural paintings, " *J. Cult. Herit*. in press.

[13]N. Schiavon, A. Candeias, T. Ferreira, M. Da Conceiçao Lopes, A. Carneiro, T. Calligaro and J. Mirao, "A combined multi-analytical approach for the study of Roman glass from south-west Iberia: Synchroton μ-XRF, external-PIXE/PIGE and BSEM–EDS," *Archaeometry*, **54**, 974–96 (2012).

[14]H. Verweij and W. L. Konijnendijk, ''Structural Units in K_2O–PbO–SiO_2 Glasses by Raman Spectroscopy,'' *J. Am. Ceram. Soc*., **59**, 517–21 (1976).

[15]H. Morikawa, Y. Takagi, and H. Ohno, ‘‘Structure Analysis of 2PbO_ SiO_2 Glass,’’ *J. Non-Cryst. Solids*, **53**, 173–82 (1982).

[16]M. Imaoka, H. Hasegawa, and I. Yasui, ‘‘X-ray Diffraction Analysis on the Structure of the Glasses in the SystemPbO–SiO_2,’’ *J. Non-Cryst. Solids*, **85**, 393–412 (1986).

[17]P. W. Wang and L. Zhang, ‘‘Structural Role of Lead in Lead Silicate Glasses Derived from XPS Spectra,’’ *J. Non-Cryst. Solids*, **194**, 129–34 (1996).

[18]T. Takaishi,M. Takahashi, J. Jin, T. Uchino, and T. Yoko, ‘‘Structural Study on PbO–SiO_2 Glasses by X-Ray and Neutron Diffraction and ^{29}Si MAS NMR Measurements,’’ *J. Am. Ceram. Soc.*, **88**, 1591–6 (2005).

[19]D. M. Sanders and L. L. Hench, ‘‘Mechanisms of Glass Corrosion,’’ *J. Am. Ceram. Soc*., **56**, 373–7 (1973).

[20]S. Wood and J. R. Blachere, ‘‘Corrosion of Lead Glasses in Acid Media: I, Leaching Kinetics,’’ *J. Am. Ceram. Soc*., **61**, 287–92 (1978).

[21]M. Mizuno, M. Takahashi, T. Takaishi, and T. Yoko, ‘‘Leaching of Lead and Connectivity of Plumbate Networks in Lead Silicate Glasses,’’ *J. Am. Ceram. Soc*., **88**, 2908–12 (2005).

[22]F. Scholz and B. Meyer, “Electroanalytical Chemistry, A Series of Advances”, A. J. Bard and I. Rubinstein, Eds., Marcel Dekker, New York, **20**, 1–86 (1998).

[23]F. Scholz, U. Schröder, R. Gulaboski and A. Doménech-Carbó, “Electrochemistry of Immobilized Particles and Droplets,” 2nd Edit. Springer, Berlin-Heidelberg (2014).

[24]A. Doménech-Carbó, J. Labuda and F. Scholz, “Electroanalytical chemistry for the analysis of solids: characterization and classification,” (IUPAC Technical Report). *Pure Appl. Chem*., **85**, 609–31 (2013).

[25]A. Doménech-Carbó, M.T. Doménech-Carbó and V. Costa, “Electrochemical Methods in Archaeometry, Conservation and Restoration,” Monographs in Electrochemistry Series, F. Scholz, Ed. Springer, Berlin-Heidelberg, 2009.

[26]A. Doménech-Carbó, M. T. Doménech-Carbó, M. A. Peiró-Ronda and L. Osete-Cortina, “Authentication of archaeological lead artifacts using voltammetry of microparticles: the case of the *Tossal de Sant Miquel* Iberian plate,” *Archaeometry*, **53**, 1193–1211 (2011).

[27]A. Doménech-Carbó, M. T. Doménech-Carbó and M. A. Peiró-Ronda, “Dating archaeological lead artifacts from measurement of the corrosion content using the voltammetry of microparticles,” *Anal. Chem., 83*, 5639–44 (2011)

[28]A. Doménech-Carbó, M. T. Doménech-Carbó, M. A. Peiró-Ronda, I. Martínez-Lázaro and J. Barrio, “Application of the voltammetry of microparticles for dating archaeological lead using polarization curves and electrochemical impedance spectroscopy,” *J. Solid State Electrochem.*, **16**, 2349–56 (2012).

[29]A. Doménech-Carbó, S. Sánchez-Ramos, M. T. Doménech-Carbó, J. V. Gimeno-Adelantado, F. Bosch-Reig, D. J. Yusá-Marco and M. C. Saurí-Peris, "Electrochemical determination of the Fe(III)/Fe(II) ratio in archaeological ceramic materials using carbon paste and composite electrodes," *Electroanalysis*, **14**, 685–96 (2002).

[30]A. Doménech-Carbó, M. T. Doménech-Carbó, M. Moya_Moreno, J. V. Gimeno-Adelantado and F. Bosch-Reig, "Voltammetric identification of lead (II) and (IV) in mediaeval glazes in abrasion-modified carbon paste and polymer film electrodes. Application to the study of alterations in archaelogical ceramic," *Electroanalysis*, **12**, 120–7 (2000).

[31]A. Doménech-Carbó, M. T. Doménech-Carbó and L. Osete-Cortina, "Identification of manganese(IV) centers in archaeological glass using micro-sample coatings attached to polymer film electrodes," *Electroanalysis*, **13**, 927–35 (2001).

[32]Doménech, A.; Doménech, M.T.; Mas, X. *Talanta* **2007**, *71*, 1569-1579.

[33]R. H. Brill, "Scientific investigation of some glasses from Sedeinga," *J. Glass Stud*. **34**, 11–29 (1991).

[34]A. M. Shugar, "Byzantine opaque red glass tesserae from Belt Shean, Israel," *Archaeometry* **42**, 375–384 (2000).

[35]Pavlov, D.; Monakhov, B. *J. Electroanal. Chem.* **1987**, *218*, 135-153.

[36]Pavlov, D.; Monakhov, B. *J. Electrochem. Soc.* **1989**, *136*, 27-33.

[37]Cai, W.-B.; Wan, Y.-Q.; Liu, H.-T.; Zhou, W.-F. *J. Electroanal. Chem.* **1995**, *387*, 95-100.

[38]Zakharchuk, N.; Meyer, S.; Lange, B.; Scholz, F. *Croat. Chem. Acta*, **2000**, *73*, 667-704.

[39]Meyer B, Ziemer B, Scholz F (1995) *In Situ* X-Ray Diffraction Study of the Electrochemical reduction of Tetragonal Lead oxide and Orthorhombic Pb(OH)Cl Mechanically Immobilized on a Graphite Electrode. J Electroanal Chem 392: 79-83.

[40]U. Hasse, F. Scholz, Hasse U, Scholz F (2000) In situ atomic force microscopy of the reduction of lead oxide nanocrystals immobilised on an electrode surface. Electrochem Commun 3: 429-434 (2001).

[41]U. Hasse, K. Wagner, F. Scholz, *J. Solid State Electrochem.* **2004**, *8*, 842.

[42]U. Hasse, J. Nieven, F. Scholz, *J. Electroanal. Chem*. **2013**, *556*, 13.

[43]Komorsky-Lovric S, Lovric M, Bond AM (1992) Comparison of the Square-Wave Stripping Voltammetry of Lead and Mercury Following their Electrochemical or Abrasive Deposition onto a Paraffin Impregnated Graphite Electrode. Anal Chim Acta 258: 299-305.

[44]M. De Keersmaecker, M. Dowsett, R. Grayburn, D. Banerjee, A. Adriaens, In-situ spectroelectrochemical characterization of the electrochemical growth and breakdown of a lead dodecanoate coating on a lead substrate., Talanta. 132 (2015) 760–8.

[45]Verweij H, Konijnendijk WL.J. Am. Ceram. Soc.1976;59: 517.

[46]Smets BMJ.J. Non-Cryst. Solids1982;48: 423.

[47]Matson DW, Sharma SK, Philpotts JA.J. Non-Cryst. Solids1983;
58: 323.

[48]Mysen BO, Frantz JD.Contrib. Mineral. Petrol.1994;117:1.

[49]Iwamoto, N., Y. Tsunawaki and M. Miyago, "Structural Study of Vitrous and Crystalline PbO-SiO_2 System by Raman Spectroscopy", Trans. JWRI 7:149-154 (1978).

[50]Götz, J., D. Hoebbel and W. Wieker, J. Non-Cryst. Solids 20:413-(1976).

[51]Lee SK, Stebbins J.J. Phys. Chem. B2003;107: 3141.

[52]Robinet, L:, A. Bouquillon and J. Hartwig, "Correlations between Raman parameters and elemental composition in lead and lead alkali silicate glasses", J. Raman Spectr. 39:618-626 (2008).

[53]Colomban P, Treppoz F. *J. Raman Spectrosc.* 2001; **32**: 93.

[54]Robinet L, Coupry C, Eremin K, Hall C. *J. Raman Spectrosc.* 2006; **37**: 789.

[55]Burgio, L., R.J.H. Clark and S. Firth, "Raman spectroscopy as a means for the identification of plattnerite (PbO_2), of lead pigments and of their degradation products," *Analyst* **126**, 222-227 (2001).

[56]Robinet L, Coupry C, Eremin K, Hall C. *J. Raman Spectrosc.* 2006; **37**: 789.

[57]Robinet L, Coupry C, Eremin K, Hall C. *J. Raman Spectrosc.* 2006; **37**: 1278.

[58]M. Scampicchio, S. Mannino, J. Zima and J. Wang, *Electroanalysis* 2005, **17**, 1215-1221.

[59]M. Imaoka, H. Hasegawa, I.Yasui, X-ray diffraction analysis on the structure of the glasses in the system PbO-SiO2, *J. Non-Cryst. Solids* 1986, 85, 393-412.

[60]A.M. Azhra, C.Y. Zahra, *J. Non-Cryst. Solids* 1993, 155, 45-55; (c) Choi et al. *J. Non-Cryst. Solids* 1999, 246, 128-135.

[61]S. Kohara, H. Ohno, M. Tanaka, T. Usuki, H. Morita, K. Suzuya, J. Akola, L. Pusztai, "Lead silicate glasses: Binary network-former glasses with large amounts of free volume," *Phys. Rev. B* 82, 134209 (2010).

[62]M.O. Figueiredo, T.P. Silva, J.P. Veiga, A XANES study of the structural role of lead in glazes from decorated tiles, XVI to XVIII century manufacture. *Appl. Phys. A* 2006, 83, 209-211.

Table 1. Provenance, chronology and elemental composition from XRF and SEM/EDX data (expressed as weight percentage of the corresponding oxides) of the archaeological lead glass samples studied. n.d.: non-detected.

Sample no.	Reference	Na_2O	MgO	Al_2O_3	SiO_2	K_2O	CaO	Fe_2O_3	CuO	PbO
S01	Puxmarina 9^{th}-10^{th}	18.47	4.76	4.69	53.73	2.08	7.72	0.90	1.66	4.49
S02	Id.	9.84	2.03	3.90	45.13	1.11	4.61	0.46	4.23	27.25
S03	Id.	14.39	3.03	1.91	51.39	1.83	4.93	2.26	2.05	17.14
S04	Reus 18^{th}	12.46	0.20	0.64	69.17	0.71	13.73	0.23	0.05	1.46
S05	Burgo de Osma 18^{th}	0.09	0.03	0.21	59.22	15.79	0.13	0.15	0.01	24.02
S06	Id.	0.25	0.11	0.48	58.94	15.73	0.38	0.20	0.02	23.51
S07	León, 13^{th}-14^{th}	0.17	3.38	1.40	46.89	22.75	21.28	2.49	0.05	0.76
S08	Goyeneche, 19^{th}	9.10	0.23	1.65	67.27	1.74	13.08	2.04	n.d.	3.70
S09	Id.	5.86	n.d.	0.42	60,26	2.80	14.24	2.55	0.87	10.29
S10	La Granja, 20^{th}	3.44	n.d.	n.d.	54.80	10.64	0.03	0.02	0.02	30.46
S11	l'Almoina, 13^{th}-15^{th}	17.1				0.80				
S12	Id.	15.7				0.34				
S13	Manises, 16^{th}-17^{th}	8.88				8.30				
S14	Paterna, 15^{th}-16^{th}	15.60				3.20				
S15	Boatella, 2^{th}									

Figures

Figure 1. Image of a sample from Puxmarina (Murcia, Spain), an iridescent fragment of lead glass from the *Andalusí* period dated back in the 9^{th}-10^{th} century.

Figure 2. Na_2O content vs. K_2O content for lead glasses in this study.

Figure 3. a) Cyclic voltammograms and b) detail of their semi-derivative convolution curves for three independent replicate experiments at S05-modified graphite electrodes immersed into air-saturated 0.25 M HAc/NaAc aqueous buffer at pH 4.75. Potential scan rate 50 mV s^{-1}.

Figure 4. Square wave voltammograms of samples a,b) S01 and c,d) S03 attached to graphite electrodes in contact with air-saturated 0.25 M HAc/NaAc aqueous buffer at pH 4.75. Potential scan initiated at a,c) +1.25 V in the negative direction; b,d) –1.25 V in the positive direction; potential step increment 4 mV; square wave amplitude 25 mV; frequency 5 Hz.

Figure 5. AFM amplitude error channel graphs of deposits of samples a) SP01 and b) SP05 on a graphite plate in contact with 0.25 M sodium acetate buffer, pH 4,75, a,c) before, and b,d) after application of a constant potential of –0.70 V for 3 min. Continuous arrows: original glass grains; dotted arrows: deposits of metallic lead of different types electrochemically generated.

Figure 6. FESEM images of deposits of samples a) SP01 and b) SP05 on a graphite plate in contact with 0.25 M sodium acetate buffer, pH 4,75, a,c) before, and b,d) after application of a constant potential of –0.70 V for 3 min.

Figure 7. Raman spectra of samples a) S08, b) S05, c) S06, d) S01, e) S03, f) S02 and g) synthetic glass 71PbO.

Figure 8. Raman spectrum of lead alkali silicate glass samples: a) S02 and b) S08, curve-fitted with decomposition model.

Figure 9. Detail of cyclic voltammograms, after semi-derivative convolution, of graphite electrodes modified with samples a) S11, b) S12; c) S13; d) S04; e) S08; f) S09 in contact with air-saturated 0.25 M HAc/NaAc aqueous buffer at pH 4.75. Potential scan rate 50 mV s^{-1}.

Figure 10. Detail of cyclic voltammograms, after semi-derivative convolution, of graphite electrodes modified with samples a) S05, b) S06; c) S07; d) S10; in contact with air-saturated 0.25 M HAc/NaAc aqueous buffer at pH 4.75. Potential scan rate 50 mV s^{-1}.

Figure 11. Detail of cyclic voltammograms, after semi-derivative convolution, of graphite electrodes modified with samples a) S01, b) S02; c) S03 and d) synthetic glass 71PbO, in contact with air-saturated 0.25 M HAc/NaAc aqueous buffer at pH 4.75. Potential scan rate 50 mV s^{-1}.

Figure 12. Two-dimensional diagram from voltammetric data such as in Figs. 6 and 7. Plots of the ratio between the current at the −600 mV peak and the maximum current in the C_{PbOx} group of peaks, $i(-600)/i(max)$, vs. the ratio between the main anodic peak and the above maximum current, $i(A_{Pb})/i(max)$ for samples in this study.

Figure 13. Dendrogram corresponding to the hierarchical cluster analysis of voltammetric data for lead glasses in this study.

Figure 14. Variation of the ratio between the intensities of the bands at 515 and 950 cm^{-1}, $I(515)/I(950)$ (squares), and the ratio between the peak currents for the $C_{Pb(IV)}$ and the maximum current in the C_{PbOx} group of peaks, $i(Pb(IV))/i(PbOx)$ (solid squares), from square wave voltammograms such as in Figure 4 vs. the Pb loading in the glass samples S01 to S10 and the synthetic glass 71PbO.

Figure 1.

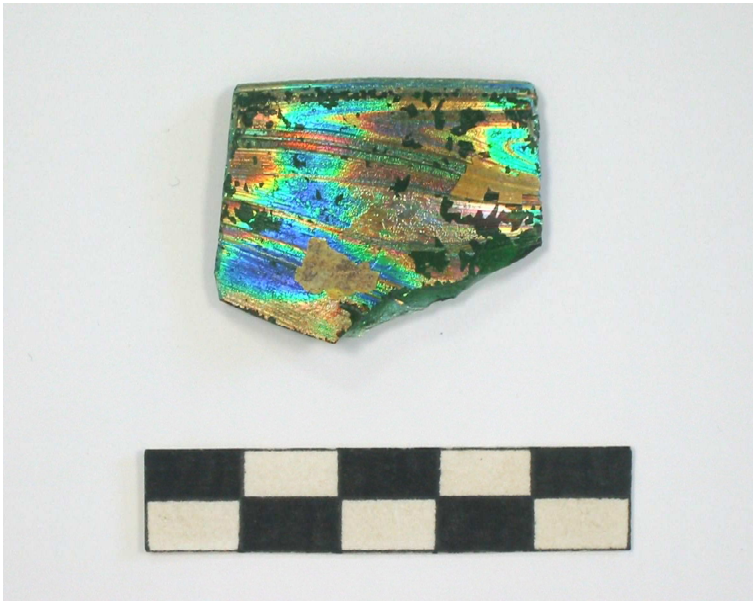

Figure 2.

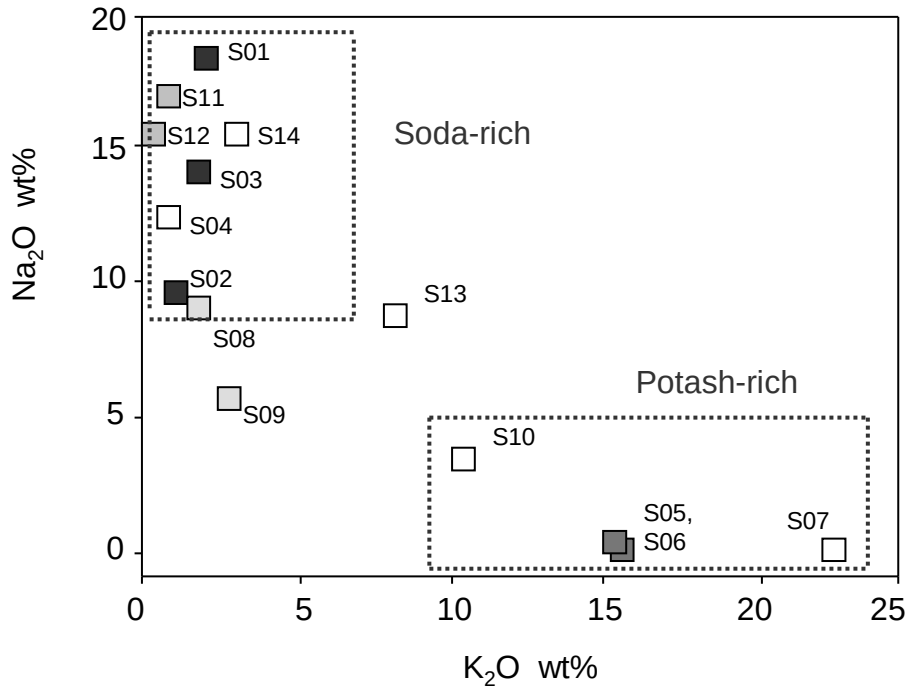
20
15
10
5
0
0
5
10
15
20
25
Na2O wt%
K2O wt%
S01
S11
S12
S14
S03
S04
S02
S08
S09
S13
S10
S05,
S06
S07
Soda-rich
Potash-rich

Figure 3.

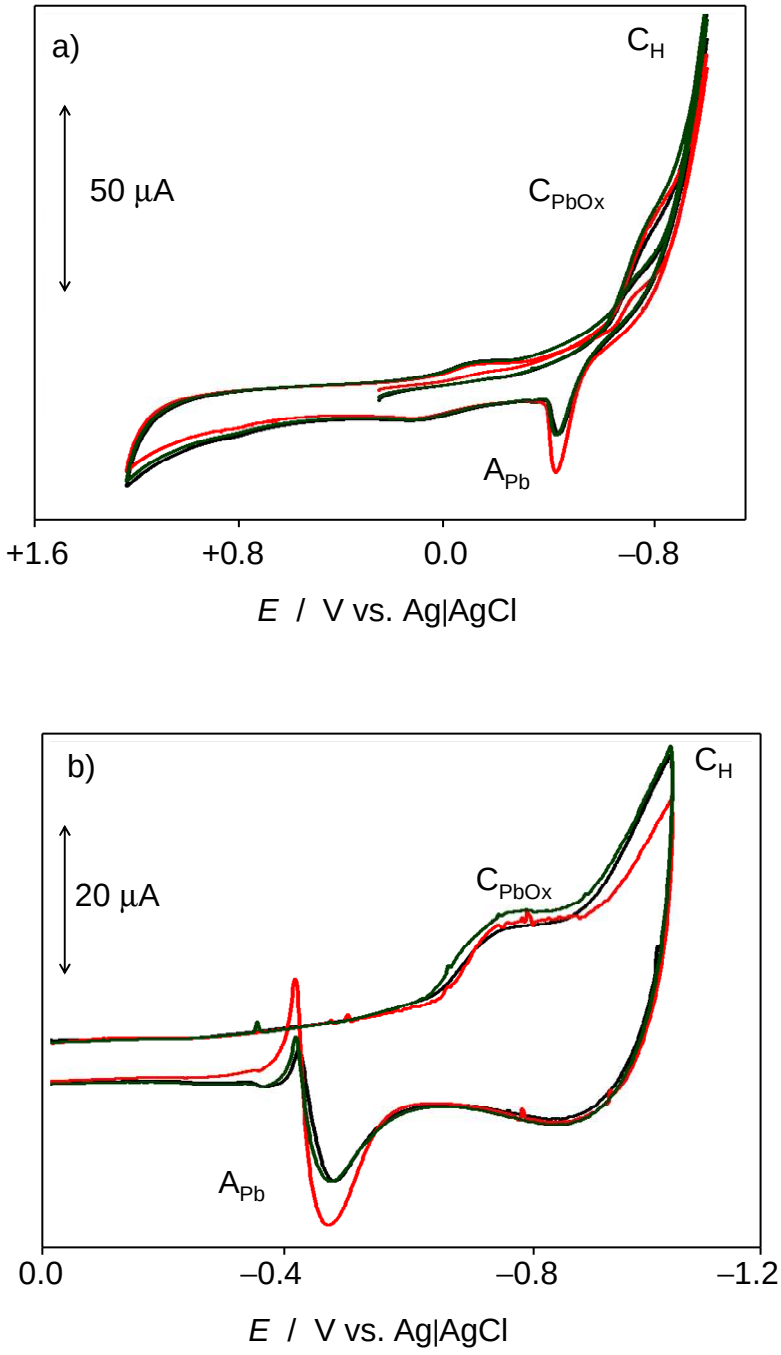
a)
C_H
50 µA
C_{PbOx}
A_{Pb}
+1.6
+0.8
0.0
–0.8
E / V vs. Ag|AgCl
b)
C_H
20 µA
C_{PbOx}
A_{Pb}
0.0
–0.4
–0.8
–1.2
E / V vs. Ag|AgCl

Figure 4.

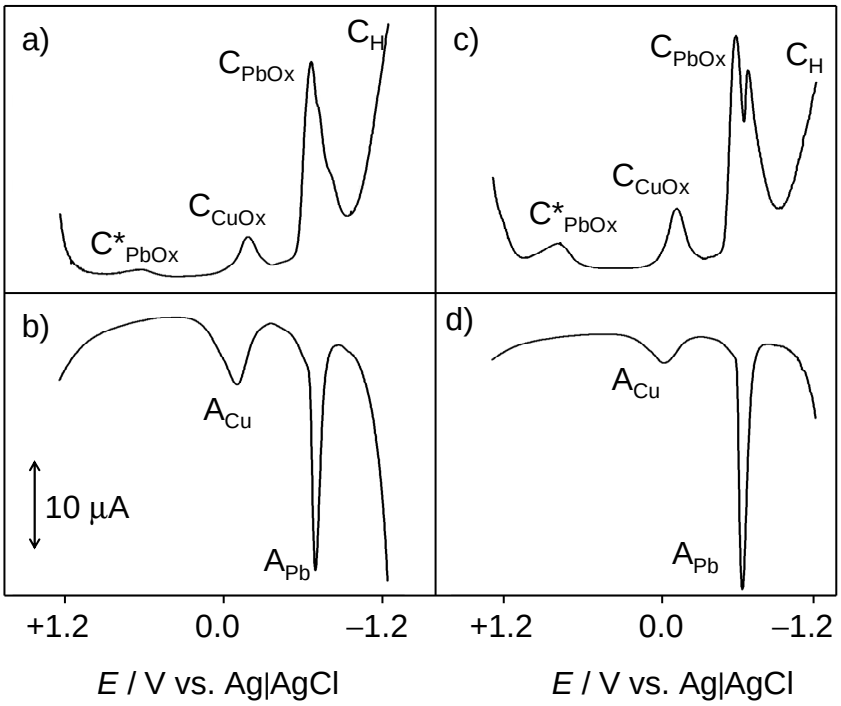
a)
C_H
C_{PbOx}
C_{CuOx}
C^*_{PbOx}
c)
C_{PbOx}
C_H
C_{CuOx}
C^*_{PbOx}
b)
A_{Cu}
10 µA
A_{Pb}
d)
A_{Cu}
A_{Pb}
+1.2
0.0
–1.2
+1.2
0.0
–1.2
E / V vs. Ag|AgCl
E / V vs. Ag|AgCl

Figure 5.

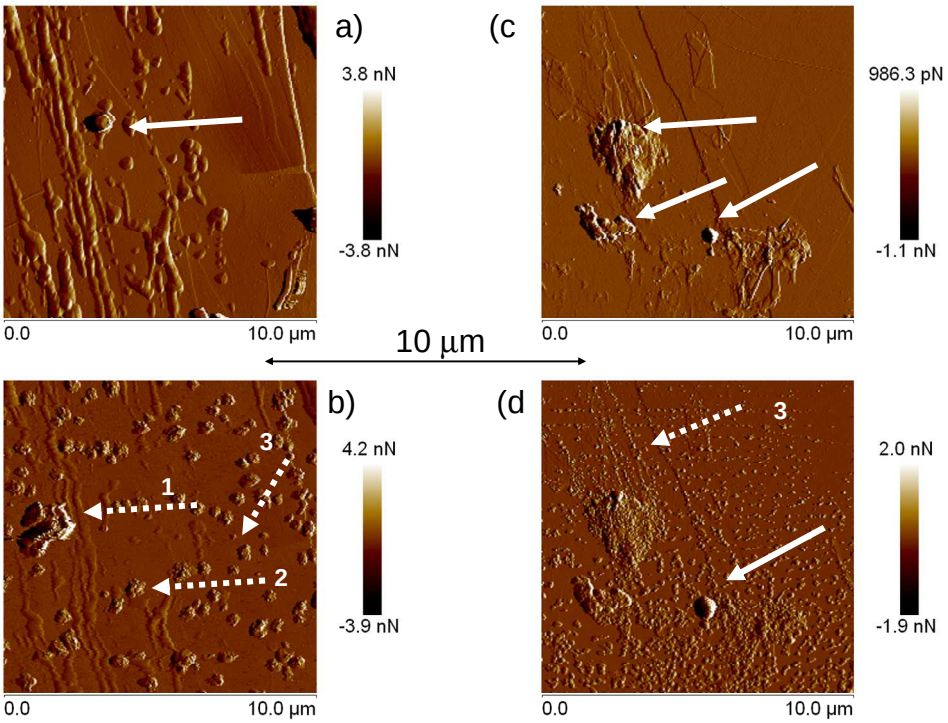
a)
3.8 nN
-3.8 nN
0.0
10.0 µm
(c
986.3 pN
-1.1 nN
0.0
10.0 µm
10 µm
b)
4.2 nN
-3.9 nN
1
2
3
0.0
10.0 µm
(d
2.0 nN
-1.9 nN
3
0.0
10.0 µm

Figure 6.

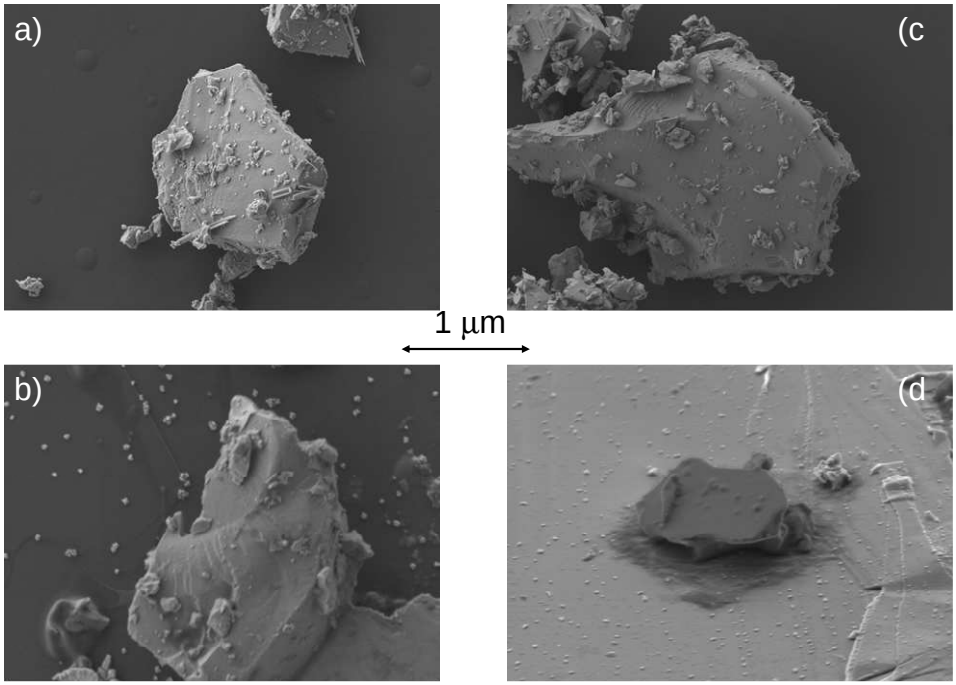

Figure 7.

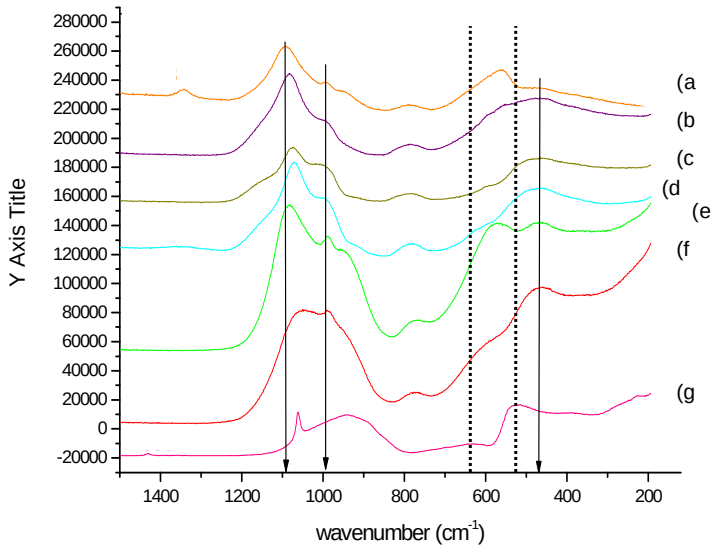
Y Axis Title
280000
260000
240000
220000
200000
180000
160000
140000
120000
100000
80000
60000
40000
20000
0
-20000
1400
1200
1000
800
600
400
200
wavenumber (cm-1)
(a
(b
(c
(d
(e
(f
(g

Figure 8.

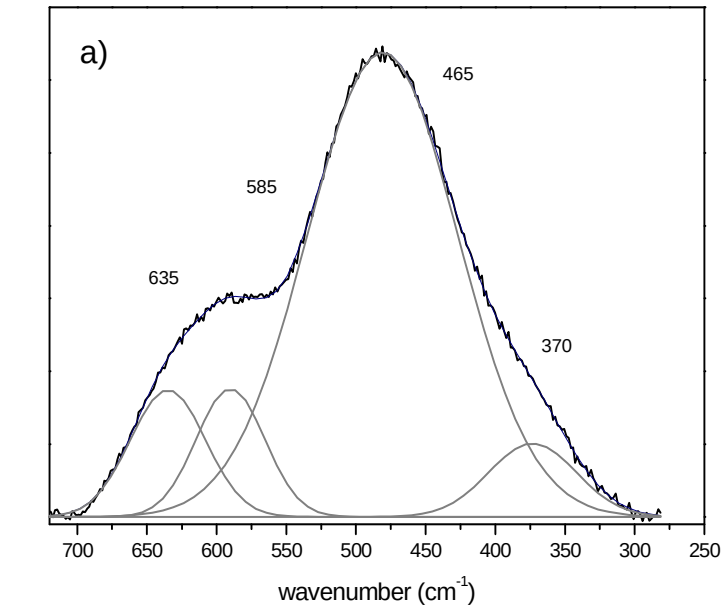
a)
465
585
635
370
700
650
600
550
500
450
400
350
300
250
wavenumber (cm-1)

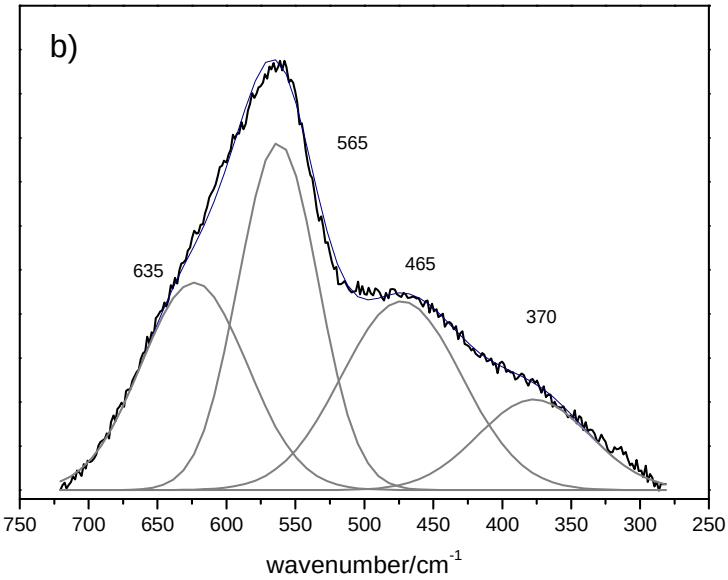
b)
565
635
465
370
750
700
650
600
550
500
450
400
350
300
250
wavenumber/cm-1

Figure 9.

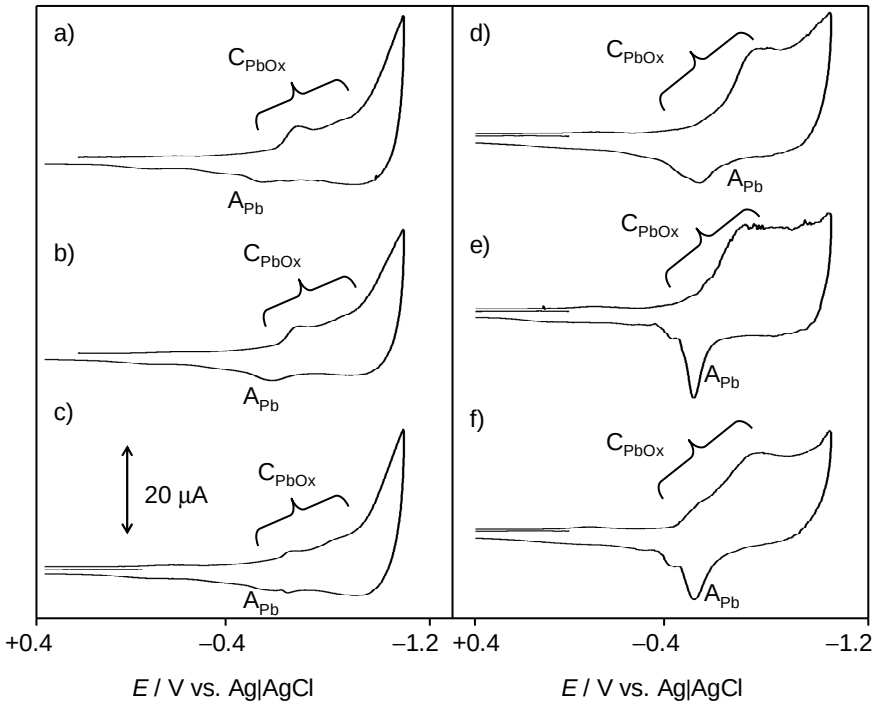
a)
C_{PbOx}
A_{Pb}
b)
C_{PbOx}
A_{Pb}
c)
20 µA
C_{PbOx}
A_{Pb}
d)
C_{PbOx}
A_{Pb}
e)
C_{PbOx}
A_{Pb}
f)
C_{PbOx}
A_{Pb}
+0.4
–0.4
–1.2
+0.4
–0.4
–1.2
E / V vs. Ag|AgCl
E / V vs. Ag|AgCl

Figure 10.

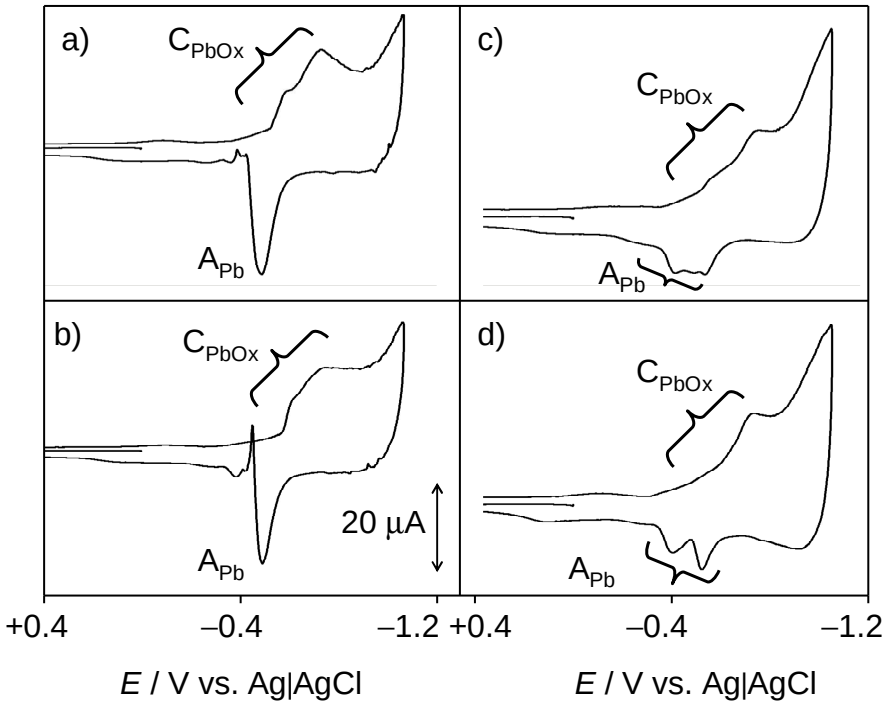
a)
C_{PbOx}
A_{Pb}
c)
C_{PbOx}
A_{Pb}
b)
C_{PbOx}
20 µA
A_{Pb}
d)
C_{PbOx}
A_{Pb}
+0.4
–0.4
–1.2
+0.4
–0.4
–1.2
E / V vs. Ag|AgCl
E / V vs. Ag|AgCl

Figure 11.

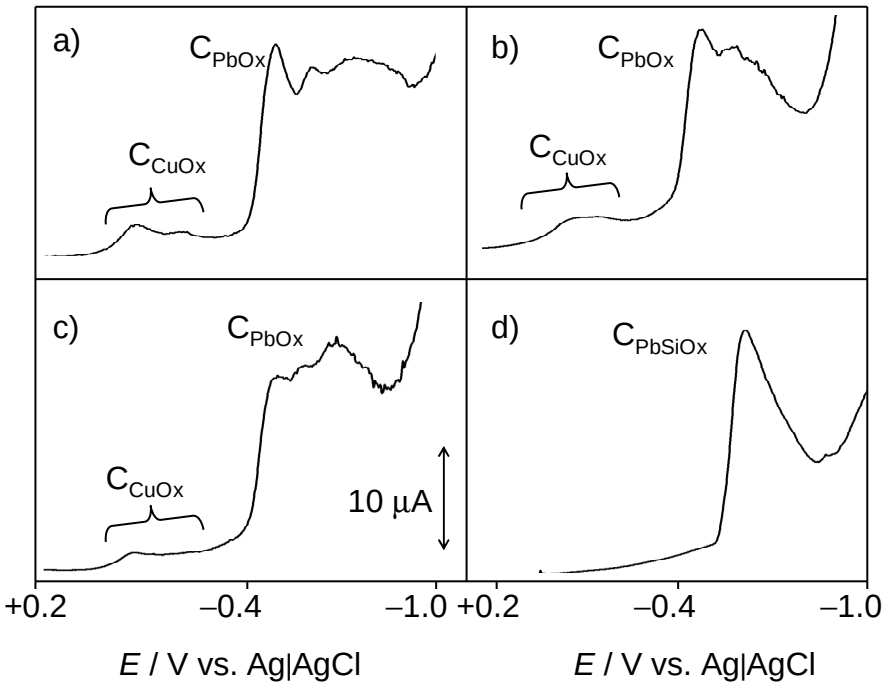
a)
C_{PbOx}
C_{CuOx}
b)
C_{PbOx}
C_{CuOx}
c)
C_{PbOx}
C_{CuOx}
10 µA
d)
C_{PbSiOx}
+0.2
–0.4
–1.0
+0.2
–0.4
–1.0
E / V vs. Ag|AgCl
E / V vs. Ag|AgCl

Figure 12.

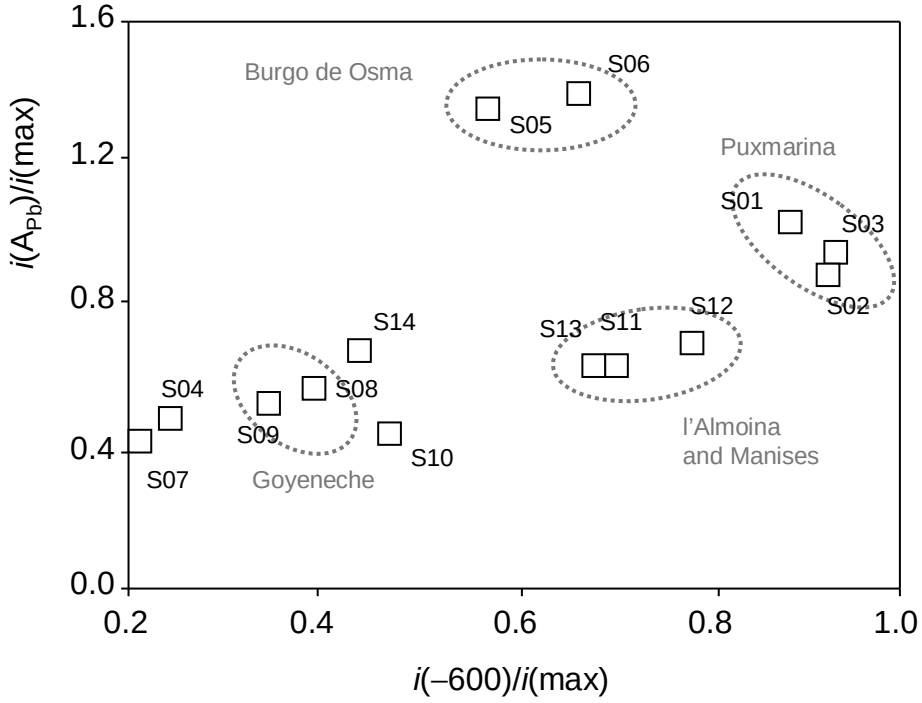
1.6
1.2
0.8
0.4
0.0
0.2
0.4
0.6
0.8
1.0
$i(A_{Pb})/i(max)$
$i(-600)/i(max)$
Burgo de Osma
S06
S05
Puxmarina
S01
S03
S02
S14
S13
S11
S12
S04
S08
S09
S10
S07
Goyeneche
l'Almoina
and Manises

Figure 13.

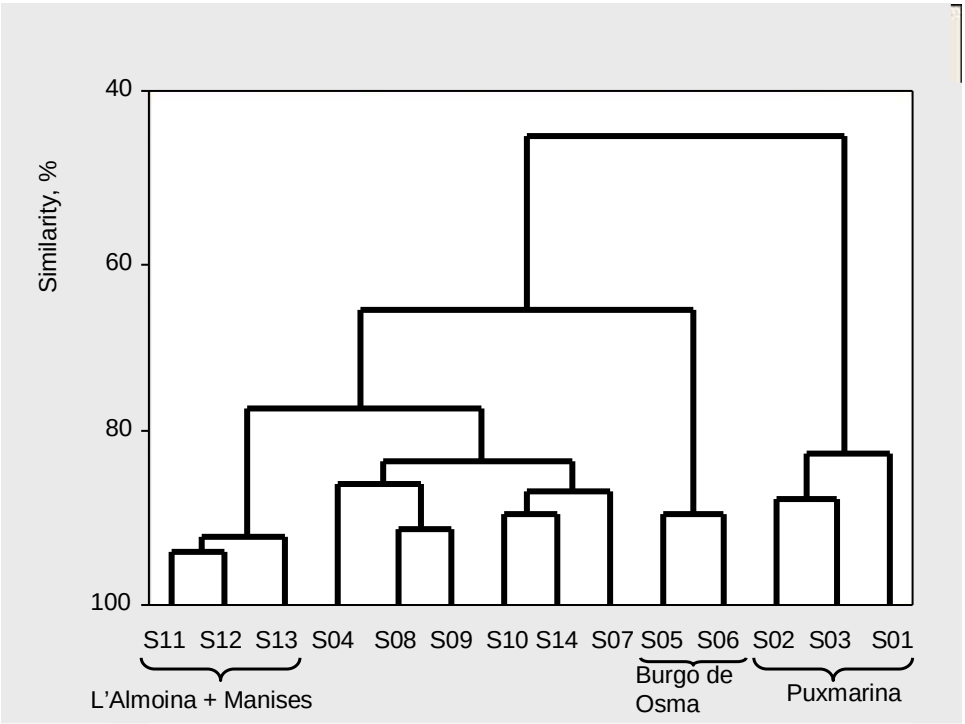
Similarity, %
40
60
80
100
S11 S12 S13 S04 S08 S09 S10 S14 S07 S05 S06 S02 S03 S01
L'Almoina + Manises
Burgo de Osma
Puxmarina

Figure 14.

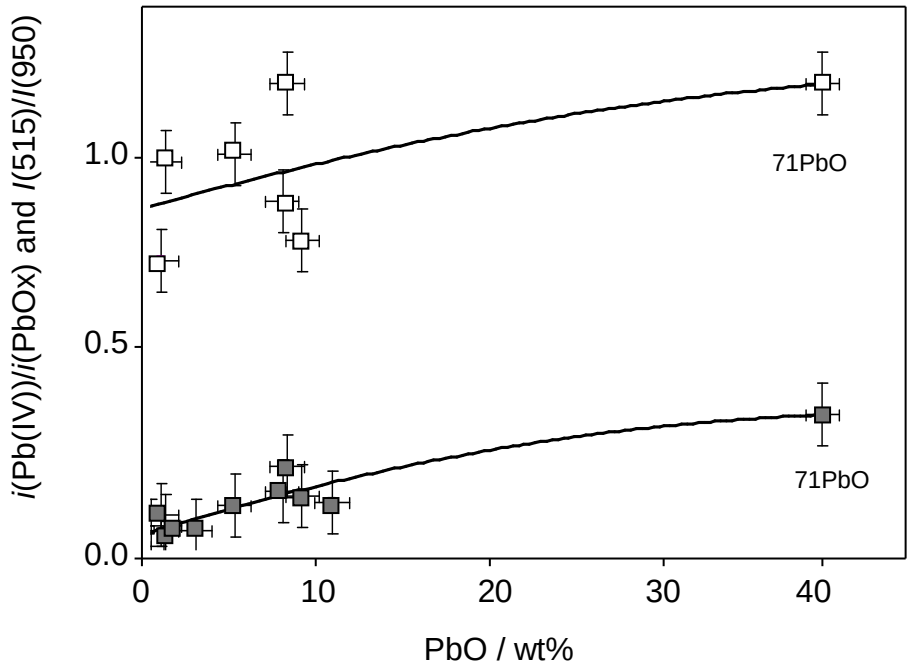
i(Pb(IV))/*i*(PbOx) and *I*(515)/*I*(950)
1.0
0.5
0.0
0
10
20
30
40
PbO / wt%
71PbO
71PbO